Nanoscale

MINIREVIEW

View Article Online
View Journal | View Issue

Cite this: *Nanoscale*, 2021, **13**, 3454

Overcoming thermal quenching in upconversion nanoparticles

Yanze Wang, †[a,b] Bing Chen †[a,b] and Feng Wang *[a,b]

Received 4th December 2020,
Accepted 15th January 2021

DOI: 10.1039/d0nr08603g

rsc.li/nanoscale

Thermal quenching that is characterized by loss of light emission with increasing temperature is widely observed in luminescent materials including upconversion nanoparticles, causing problems in technological applications such as lighting, displays, and imaging. Because upconversion processes involve extensive intra-particle energy transfer that is temperature dependent, methods have been established to fight against thermal quenching in upconversion nanoparticles by engineering the energy transfer routes. In this minireview, we discuss the origin of thermal quenching and the role of energy transfer in thermal quenching. Accordingly, recent efforts in overcoming thermal quenching of upconversion are summarized.

1. Introduction

Luminescent materials have been playing important roles in a variety of modern technologies such as lasers, displays, and solar energy conversion.[1] As a unique class of luminescent materials, lanthanide-doped upconversion nanoparticles (UCNPs) are particularly useful for biomedical and photonic applications due to their ability to generate visible and ultraviolet emissions by excitation of near-infrared light, which is less absorbed and scattered than the conventional ultraviolet excitation light.[2–10] Due to their advantages of a large anti-Stokes frequency shift, high chemical stability, sharp emission peak, and low toxicity, UCNPs excel in many aspects than other types of optical materials such as quantum dots and organic dyes.[11–15]

In practical applications, a luminescent component should display bright emission that is stable against variations in the environment such as temperature. However, most luminescent materials show attenuation of emission intensity with the increase in the temperature, which is well known as thermal quenching.[16–18] Typically, thermal quenching in UCNPs is more complicated and severe than that in relevant Stokes shifting luminescent materials because the multiple excited states involved in the upconversion process are all subjected to thermal deactivation (Fig. 1).[19–40] The problem has stimulated considerable research interest in combating thermal quenching in UCNPs.[41]

In this minireview, we focus on recent advances in the development of UCNPs that are resistant to thermal quenching. In section 2, we discuss various thermal quenching mechanisms and their influence on lanthanide-based upconversion. Accordingly, recent efforts in overcoming thermal quenching are reviewed in section 3.

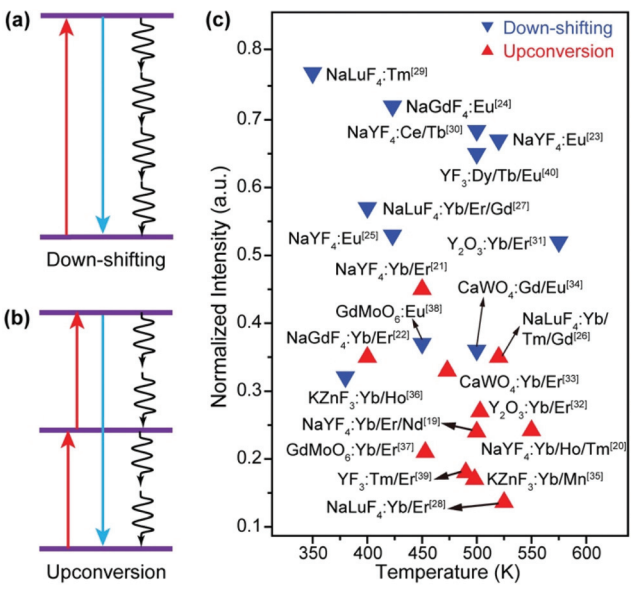

Fig. 1 Schematic illustration of nonradiative quenching in (a) down-shifting and (b) upconversion luminescence processes. (c) Reported relative emission intensity as a function of temperature in typical inorganic luminescent materials, demonstrating the higher susceptibility of upconversion to thermal quenching than relevant down-shifting luminescence. The emission intensities at the room temperate are set as unity.

[a]*Department of Materials Science and Engineering, City University of Hong Kong, 83 Tat Chee Avenue, Hong Kong SAR, China. E-mail: fwang24@cityu.edu.hk*
[b]*City University of Hong Kong Shenzhen Research Institute, Shenzhen 518057, China*
† These authors contributed equally to this work.

2. The origin of thermal quenching

Thermal quenching of luminescence results from the increased dissipation of excitation energy at elevated temperatures, which can be due to the prevalence of nonradiative relaxations in individual luminescent centres and enhancement of interionic processes involving electron and energy transfer (Fig. 2).

2.1 Thermal quenching in individual luminescent centres

Apart from emitting light, an excited luminescent centre has several possible deactivation channels, such as multiphonon relaxation, crossover and thermal ionization (Fig. 2a–c). In general, these nonradiative processes are enhanced with an increase in temperature due to the increased vibrational energy of the host lattice, thereby leading to increased loss of light emission.

Multiphonon relaxation is a quenching process in which the energy gap (ΔE_m) between the excited state and the next lower-lying state is bridged by simultaneously emitting phonons (Fig. 2a).[42–45] The probability of multiphonon relaxation (K_{nr}) is dependent on ΔE_m and phonon energy ($\hbar\omega$) in the host lattice as described by eqn (1)[46]

$$K_{nr} \propto \exp\left(-\beta \frac{\Delta E_m}{\hbar\omega}\right) \quad (1)$$

where β is an empirical constant of the host. Multiphonon relaxation can occur at low temperatures. However, the multiphonon transition rate increases with the increase in temperature, because the thermally populated phonon modes in the host lattice can induce stimulated emission of phonons.[47]

Crossover is a thermally activated process in which electrons at the excited energy level jump over the intersection between the excited state and the ground state parabola by overcoming an energy barrier (ΔE), followed by nonradiative relaxation to the ground state (Fig. 2b).[48] The probability of crossover is strongly dependent on the polyhedral average bond length difference between the excited state and the ground state (ΔR). A large ΔR results in a small ΔE and thus a strong thermal quenching effect.

Thermal ionization involves the ejection of electrons from the localized excited state to the conduction band (CB) of the host material, as shown in Fig. 2c.[49] After thermal stimulation, the ionized electrons often recombine nonradiatively with the photo-oxidized luminescent centre. Alternatively, the ionized electrons may be captured by traps in the host (*e.g.*, substitutional impurity atoms, vacancies and anti-site defects), followed by various relaxation processes.[50] In both cases, the light output from the original luminescent centre is reduced.

Electronic transitions in lanthanide dopant ions primarily occur within the 4f orbital that is shielded by the 5s and 5p orbitals, resulting in extremely small changes in the polyhedral average bond length. Therefore, direct thermal quenching in upconversion centres is mainly induced by multiphonon relaxation.

2.2 Thermal quenching due to interionic processes

In addition to intra-ionic transitions, a luminescent ion may lose its excitation energy to an adjacent optical centre by electron or energy transfer (Fig. 2d–f), which is typically enhanced by thermal energy and eventually leads to the quenching of emission.

Optical quenching by electron transfer is illustrated in Fig. 2d for a system comprising two species A and B, which involves a ground state (A + B), an excited state (A* + B), and a charge transfer (CT) state ($A^+ + B^-$).[51–53] The CT state bridges

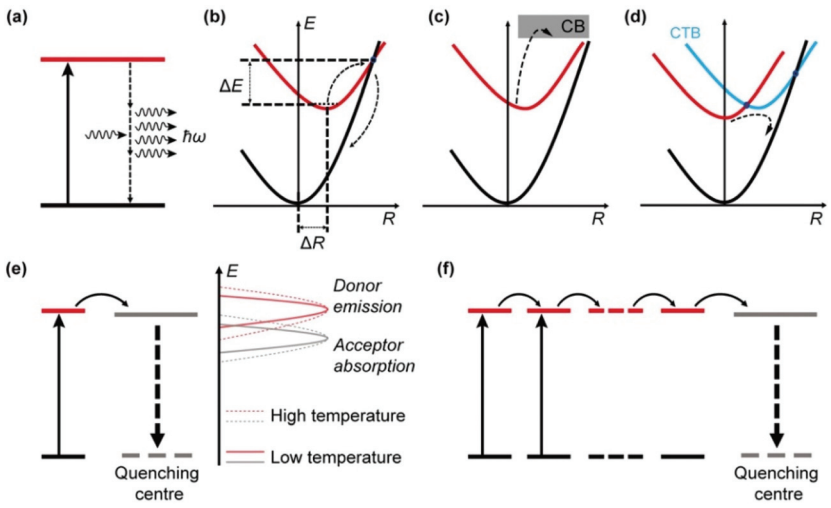

Fig. 2 Summary of thermal quenching mechanisms in inorganic luminescent materials. (a) Multiphonon relaxation that can be stimulated by phonon modes in the host lattice. (b) Configurational coordinate (R) diagram illustrating the thermally activated crossover quenching process. (c) Configurational coordinate diagram of the thermal ionization process, in which electrons were directly excited into the conduction band (CB). (d) Configurational coordinate diagram showing quenching through the charge transfer band (CTB). (e) Nonradiative decay due to energy transfer to a quenching centre, which strengthens with the increase in temperature. (f) Optical quenching due to energy hopping through the dopant sublattice.

the excited state and ground state in a process that resembles crossover, leading to quenching of the emission. CT typically occurs between two optical centres with opposite redox tendencies (*e.g.*, Eu^{3+} and Ce^{3+}),[54–56] which results in a low CT state energy favourable for the crossover to proceed.

The principle of energy transfer between two species was developed by Förster and Dexter.[57,58] The probability of energy transfer (P_{ET}) largely depends on spectral overlap between the energy donor and acceptor pairs according to eqn (2).[58,59]

$$P_{ET} \propto \int f_D(E) f_A(E) dE \quad (2)$$

where $f_D(E)$ and $f_A(E)$ are normalized shape functions of the donor emission and acceptor absorption over energy (E), respectively. Due to thermal broadening of the spectrum as a result of vibronic coupling, spectral overlap typically improves with an increase in temperature, leading to enhancement of energy transfer (Fig. 2e).[60] Thermal energy also promotes energy transfer processes by making up the energy mismatch between the energy donor and acceptor.[61]

UCNPs typically comprise a large number of lanthanide dopant ions (*e.g.*, Yb^{3+}) that undergo extensive energy transfer interactions in the host lattice. Consequently, a lanthanide ion that is far from a quenching centre may be affected following multiple energy transfer steps (energy hopping) through the dopant sublattice (Fig. 2f).[62,63] The energy hopping process exhibits a complex dependency on temperature and can be harnessed to manipulate the thermal quenching process.

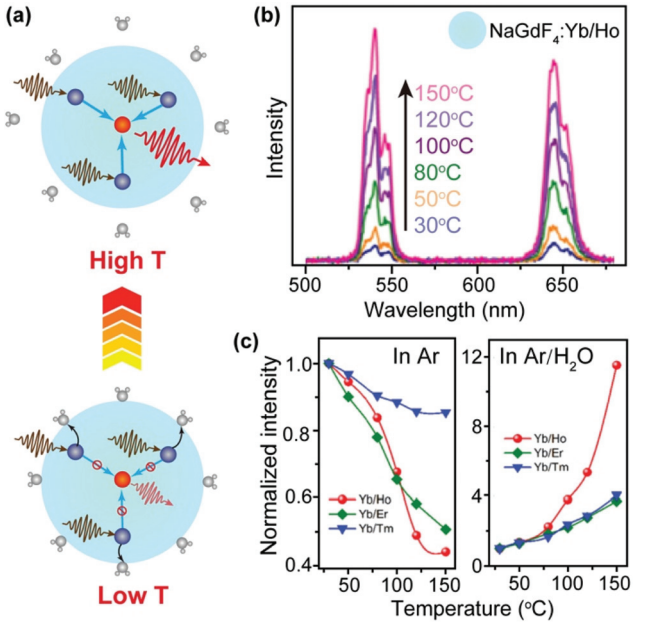

Fig. 3 (a) Schematic diagram of temperature-dependent energy exchange interactions between sensitizer and activator ions as well as between sensitizer ions and surface H_2O molecules in UCNPs. The navy and red spheres represent sensitizers and activators, respectively. (b) Emission spectra of $NaGdF_4$:Yb/Ho (20/2%) nanoparticles in the temperature range of 30–150 °C. (c) Integral emission intensities of $NaGdF_4$:Yb/Ho (or Er, Tm) (20/2%) nanoparticles as a function of temperature under Ar and Ar/H_2O atmospheres, respectively. The intensities were normalized to those at 30 °C. Reproduced with permission from ref. 70. Copyright 2018, American Chemical Society.

3. Recent efforts in overcoming thermal quenching

Nonradiative relaxation processes in individual luminescent centres can hardly be alleviated as the temperature increases. Attempts to overcome thermal quenching are thus mainly based on the suppression of energy transfer to quenching sites at high temperatures. Because the luminescent centres (or activators) in UCNPs also receive energy from sensitizers (*e.g.*, Yb^{3+} co-dopants), the effect of thermal quenching may alternatively be offset by thermal enhancement of the sensitization process.

3.1 Thermal alleviation of energy dissipation

Nanoparticles are characterized by large surface-to-volume ratios and most quenching processes occur at the nanoparticle surface. In particular, surface absorbed water molecules induce significant quenching of upconversion emission by introducing high energy oscillation modes such as O–H vibration.[64]

An increase in temperature typically induces desorption of water molecules and thus results in the alleviation of surface quenching, which offset thermal quenching and may eventually lead to enhancement of upconversion emission at elevated temperatures (Fig. 3a). The major origin of the energy loss in UCNPs is the strong interaction between heavily doped sensitizer ions (*e.g.*, Yb^{3+}) and high-energy oscillations of H_2O molecules.[65–68] In addition to multiphonon relaxation, the dopants may also be coupled to overtone transition of H_2O molecules.[69] Owing to the elimination of water-induced surface quenching, Jiang and co-workers observed a 12.6-fold enhancement of upconversion emission from $NaGdF_4$:Yb/Ho (20/2%) nanoparticles under an Ar/H_2O atmosphere as the temperature increased from 30 to 150 °C (Fig. 3b).[70] The control experiment revealed that the luminescence was thermally quenched under a dry Ar atmosphere (Fig. 3c and d), which validated the role of water desorption for enhancing upconversion luminescence. The thermal enhancement process was reversible and can also be realized in $NaGdF_4$:Yb/Er (or Tm) (20/2%) nanoparticles. A similar result was reported by Meijerink and co-workers, who observed a 3-fold thermal enhancement of integral upconversion emission of Er^{3+} ions in $NaY(WO_4)_2$:Yb/Er (49/1%) nanoparticles from 330 to 470 K under an ambient atmosphere.[71] By contrast, thermal quenching of upconversion emission was observed in dry N_2.

In a follow-up study, Jiang and co-workers reported wavelength-selective enhancement of upconversion in $NaGdF_4$:Yb/Ce/Ho (20/30/2%) nanoparticles due to water desorption at elevated temperatures.[72] Under 975 nm excitation, the green and red emission intensities at 450 K were about 1.7- and 10.2-fold stronger than those at 300 K, respectively. As a result, the

emission colour clearly shifted from green to red with the increase in temperature, which was attributed to a thermally enhanced cross-relaxation between Ho^{3+} and Ce^{3+} ions. Notably, continuous laser irradiation was found to induce a heating effect, which can result in water desorption and thus modulation of upconversion emission.

Surface quenching may also affect dopant ions in the interior of the nanoparticles *via* energy migration.[73–76] An increase in temperature normally causes the expansion of the host lattice, which hampers the long-distance energy migration process and consequently alleviates the quenching process (Fig. 4a). In an early example, Wang and co-workers described an anomalous temperature-dependence of upconversion luminescence in $NaGdF_4$:Yb/Eu (20/10%) nanoparticles, which was related to energy migration through the sublattice of Yb^{3+} sensitizers.[77] As a result of suppressed energy migration, a 16-fold enhancement of upconversion emission in Eu^{3+} ions ($^5D_0 \rightarrow {}^7F_2$ transition) was detected as the temperature increased from 303 to 423 K (Fig. 4b). In a recent study by our group, a thermal enhancement of upconversion emission was observed in oleate-capped $NaYbF_4$:Er (2%)@$NaLuF_4$:Yb (25%) UCNPs in the temperature range of 298–473 K, ascribed to lattice-expansion-induced interruption of energy migration among Yb^{3+} ions that were located in the core and active shell (Fig. 4c).[78] When surface quenching effect was eliminated using an inert $NaLuF_4$ shell, however, normal thermal quenching other than thermal enhancement of upconversion was observed in the same temperature range (Fig. 4d).

It is clear from the above discussions that the thermally enhanced upconversion in this category is essentially an emission recovery process. If the UCNPs are initially protected against surface quenching in host materials with a core–inert shell structure or a large size, thermal quenching of upconversion luminescence is generally detected.[79–83] Intriguingly, by integrating upconversion components displaying distinct thermal properties in a single nanoparticle or a nanoparticle mixture (Fig. 5a), novel systems can be constructed for applications such as thermometry[84,85] and thermochromism.[81,86–88]

In a recent example, Mi *et al.* prepared a class of $NaYF_4$:Yb/Er (20/2%)@$NaYF_4$@$NaYF_4$:Yb/Nd (60/4%) nanorods (Fig. 5b).[89] It was reported that the Yb/Nd couple at the nanorod surface showed thermally enhanced emission, while the Yb/Er couple in the core of the nanorod exhibited thermally quenched luminescence. Based on the emission intensity ratio of Nd^{3+} and Er^{3+}, sensitive nanothermometry (9.6%/K at 303 K) with a fast temperature response was demonstrated. In another development, Hu *et al.* constructed a class of thermochromic nanocomposite inks by mixing $NaGdF_4$:Yb/Tm (20/1%)@$NaGdF_4$ core–inert shell and $NaGdF_4$:Yb/Er (20/1%)@$NaGdF_4$:Yb (20%) core–active shell nanoparticles (Fig. 5c), which displayed thermally quenched and enhanced upconversion, respectively.[90] The thermochromic nanocomposite inks are potentially useful for anticounterfeiting applications.

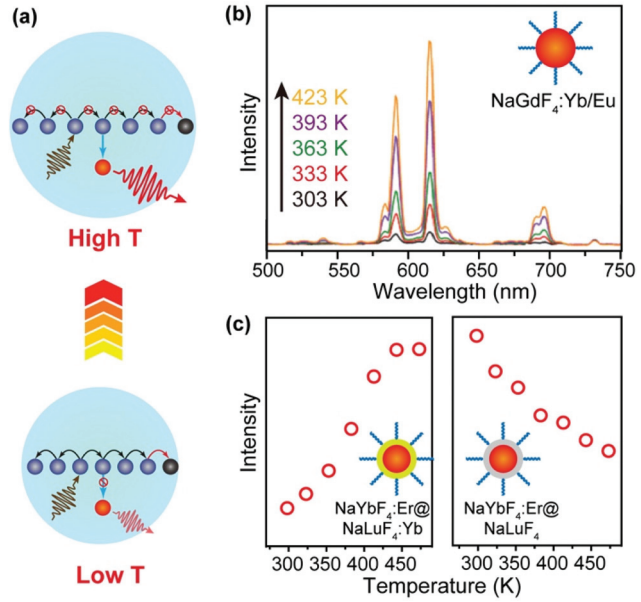

Fig. 4 (a) Thermal suppression of energy migration to surface quenchers by lattice expansion. (b) Temperature-dependent upconversion emission spectra (excitation at 980 nm) of $NaGdF_4$: Yb/Eu UCNPs with a size of 10 nm. Adapted with permission from ref. 77. Copyright 2017, Royal Society of Chemistry. (c) Emission intensities at 657 nm due to $^4F_{9/2} \rightarrow {}^4I_{15/2}$ transitions of Er^{3+} as a function of temperature in oleate-capped $NaYbF_4$:Er (2%)@$NaLuF_4$:Yb (25%) and $NaYbF_4$:Er (2%)@$NaLuF_4$ core–shell nanoparticles, respectively. Adapted with permission from ref. 78. Copyright 2019, American Chemical Society.

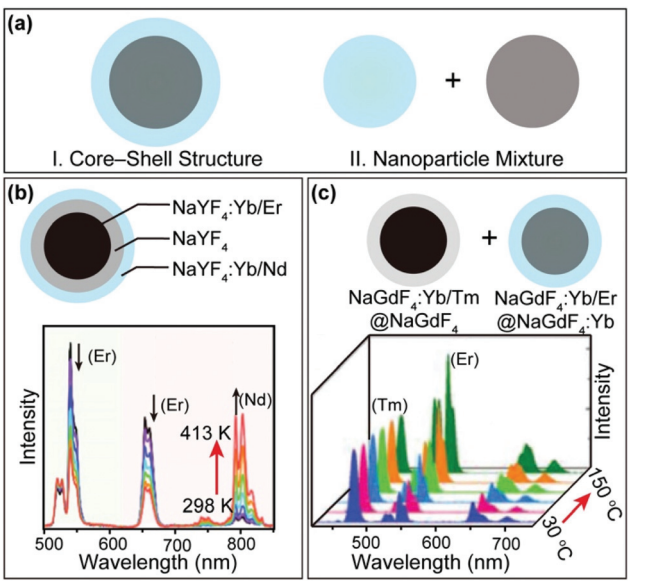

Fig. 5 (a) Schematic illustration of integrating upconversion components displaying distinct temperature dependence of luminescence. (b) Emission spectra of $NaYF_4$:Yb/Nd (20/6%)@$NaYF_4$@$NaYF_4$:Yb/Er (20/0.5%) nanorods in the temperature range of 298–413 K. Adapted with permission from ref. 89. Copyright 2019, American Chemical Society. (b) Emission spectra of $NaGdF_4$:Yb/Er@$NaGdF_4$ nanoparticles mixed with $NaGdF_4$:Yb/Er@$NaGdF_4$:Yb in the temperature range of 30–150 °C. Adapted with permission from ref. 90. Copyright 2019, Wiley-VCH.

3.2 Thermal enhancement of energy collection

A majority of upconversion processes are based on energy transfer from the sensitizer (*e.g.*, Yb^{3+}) to activator (*e.g.*, Er^{3+}) ions. Such energy transfer processes can be enhanced with the increase in the temperature, which may offset thermal quenching in activator ions and even lead to enhancement of upconversion emissions at elevated temperatures.

The energy transfer in UCNPs is usually a phonon-assisted process that is temperature dependent.[90–93] Due to the quantum confinement effect, a cut-off of low-energy phonons in UCNPs was reported at low temperatures.[94,95] Fortunately, an increase in temperature can mitigate the confinement effect, thereby promoting the energy transfer processes (Fig. 6a). In an early example, Jiang and co-workers reported thermally enhanced luminescence in small-sized $NaYF_4$:Yb/Er (20/2%) UCNPs (24 nm), which was attributed to the activation of the phonon-assisted energy transfer process.[79] The thermally activated phonons make up the energy mismatch between Yb^{3+} and Er^{3+}, thereby facilitating the energy transfer process (Fig. 6b). Under 975 nm laser excitation, the luminescence intensity of Er^{3+} in the UCNPs increased 2-fold as the temperature increased from 298 to 358 K (Fig. 6c). In another study, Zhou *et al.* reported that as the temperature increases from 300 K to 453 K the oleate-capped $NaYF_4$:Yb/Tm (49/1%) UCNPs would produce more surface phonons due to the [Yb···O] complexes, which made up the energy gap between Yb^{3+} sensitizers and Tm^{3+} activators, thereby resulting in about 2000-fold enhancement of the blue emission in Tm^{3+} ($^1G_2 \rightarrow {}^3F_4$).[96] However, due to the extremely weak emission of the UCNPs at room temperature, the enhancement effect may be overvalued. On a separate note, Shi *et al.* suggested that the thermally enhanced upconversion in these small nanoparticles may also be partly attributed to water desorption,[69] which was not examined in the original studies.

Recently, the temperature dependence of upconversion luminescence has been assessed in host materials displaying anomalous thermal contraction characteristics.[97–99] Owing to the negative thermal expansion (NTE), sensitizer–activator pairs are brought in close proximity at elevated temperatures, which favours the energy transfer process and thus promotes the upconversion emission (Fig. 7a).[100] In a pioneering study by our group, a 29-fold enhancement of green emission and a 13-fold enhancement of overall emission in $Yb_2W_3O_{12}$:Er (6%) microcrystals were achieved by increasing the temperature from 303 to 573 K (Fig. 7b).[101] The mechanistic investigation confirmed that both light absorption by the Yb^{3+} sensitizer and energy transfer to Er^{3+} activators were enhanced with the increase in temperature, owing to lattice contraction and distortion. Subsequently, thermal enhancement of upconversion luminescence was also observed in other NTE materials such as $Sc_2Mo_3O_{12}$:Yb/Ho (18/2%) microcrystals and ScF_3:Yb/Er (18/2%)@ScF_3 core–shell nanocrystals, demonstrating the versatility of the NTE effect for enhancing upconversion in a thermal field.[102,103]

It is worth noting that luminescent centres may gain energy from defect states in the host lattice at elevated temperatures, which also opposes thermal quenching. In a representative example, Kim *et al.* reported an electron loop (thermal ioniza-

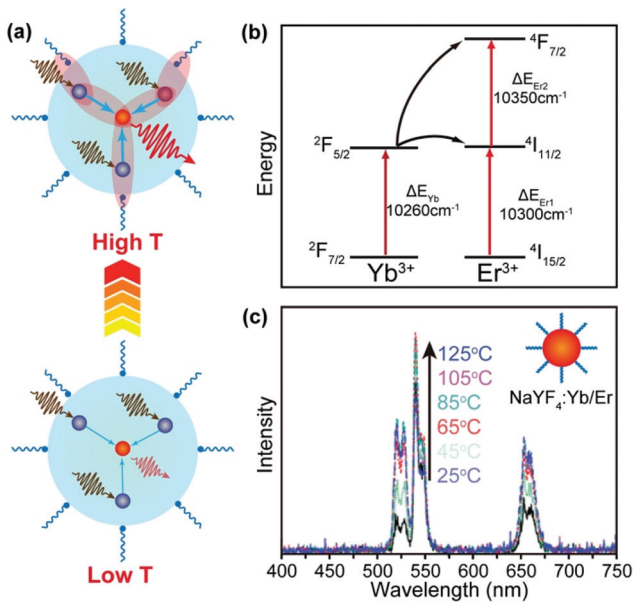

Fig. 6 (a) Thermal activation of phonon-assisted energy transfer. (b) Mismatch of energy levels between Yb^{3+} and Er^{3+} ions, illustrating the need for phonon participation in the energy transfer process. (c) Temperature-dependent upconversion emission spectra of $NaYF_4$:Yb/Er (20/2%) UCNPs (24 nm) in the temperature range of 25–125 °C. Reproduced with permission from ref. 79. Copyright 2014, American Chemical Society.

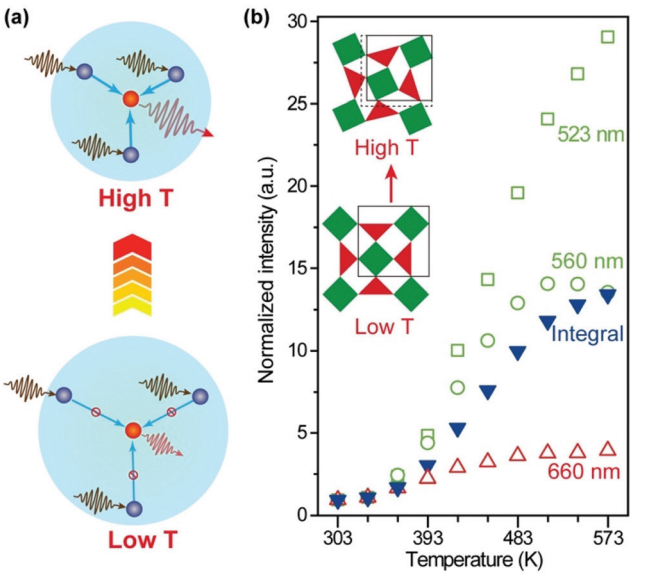

Fig. 7 (a) Thermal promotion of energy delivery to activator ions by lattice contraction in negative thermal expansion crystals. (b) Normalized emission intensities of $Yb_2W_3O_{12}$:Er (6%) nanocrystals as a function of temperature. Inset: schematic of the lattice contraction and distortion as the temperature increases. Adapted with permission from ref. 101. Copyright 2019, Wiley-VCH.

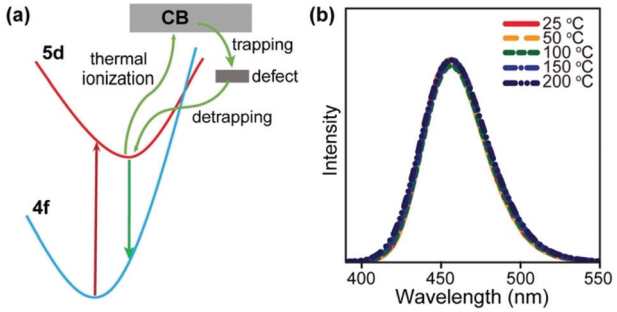

Fig. 8 (a) A simplified model for the zero-thermal-quenching due to structural defects. (b) Temperature-dependent emission spectra of $Na_3Sc_2(PO_4)_3$:Eu (divalent, 0.7%) phosphors under 370 nm excitation in the temperature range of 25–200 °C. Reproduced with permission from ref. 104. Copyright 2017, Nature Publishing Group.

tion → defect trapping → detrapping) process in $Na_3Sc_2(PO_4)_3$:Eu (divalent, 0.7%) blue-emitting phosphors to combat thermal quenching.[104] $Na_3Sc_2(PO_4)_3$ is a polymorphic material that undergoes cation disordering upon heating, leading to defect formation. The structural defects can trap thermally ionized electrons followed by energy transfer to the Eu^{2+} activators, thereby contributing to the recovery of light emission at elevated temperatures (Fig. 8). To date, such defect-assisted processes are primarily observed in down-shifting luminescent materials.[105–109] Novel designs need to be adopted in order to take advantage of the structural defects in UCNPs.

4. Conclusions

In conclusion, we have summarized various nonradiative processes and addressed their temperature dependence. Accordingly, recent efforts for alleviating energy dissipation and enhancement of energy collection have been reviewed to combat thermal quenching in UCNPs. By the rational selection of host/dopant combination coupled with precise control of the nanoparticle size and surface coating, novel UCNPs have even been constructed to display thermally enhanced upconversion emission.

Despite the achievements, the exact mechanism for these anti-thermal quenching phenomena is still a topic of debate though various explanations have been proposed by different research groups. Nanostructures often experience complex changes during heat treatment and may be subjected to chemical reactions even at moderate temperatures.[110,111] Therefore, special attention should be paid to the temperature-dependent characterization of these nanomaterials in future mechanistic investigations. On a separate note, the established UCNPs that excel in thermal fields usually display poor upconversion performances. To achieve thermal enhancement of upconversion, or more precisely thermal recovery of radiative emission, lanthanide dopant ions are typically exposed to the nanoparticle surface, leading to significant surface quenching and thus low upconversion efficiency.

Considering the extensive investigations of upconversion in $NaYF_4$ and its variants, future construction of UCNPs with high performance at both room and high temperatures may hinge on the development of new compositions and structures. One potential direction is to construct nonuniformly coated core–shell UCNPs through strain engineering,[112–115] which modifies the crystal parameters of the host lattice and alters the crystal field around the luminescent dopants. In addition, the thermal response of anisotropic core–shell UCNPs is affected by multiple factors, thereby permitting the study of competitive relationships between thermal enhancement and quenching.

NTE hosts represent another important class of materials for future exploration. The NTE effect leads to thermal modulation of upconversion irrespective of the crystal surface status,[101–103] which offers great flexibility for optimizing the luminescence efficiency. Given the large number of inorganic crystals that are found to show NTE characteristics, such as $MgZrF_6$, $CaZrF_6$ and $CaHfF_6$,[116–118] a family of new upconversion materials can be constructed to combat thermal quenching of luminescence.

Conflicts of interest

There are no conflicts to declare.

Acknowledgements

This work was supported by the National Natural Science Foundation of China (No. 21773200) and the Research Grants Council of Hong Kong (CityU 11204717 and 11205219).

Notes and references

1 G. Blasse and B. Grabmaier, *Luminescent Materials*, Springer, Berlin, 1994.
2 B. Chen, Y. Liu, Y. Xiao, X. Chen, Y. Li, M. Li, X. Qiao, X. Fan and F. Wang, *J. Phys. Chem. Lett.*, 2016, **7**, 4916–4921.
3 W. Zheng, P. Huang, D. Tu, E. Ma, H. Zhu and X. Chen, *Chem. Soc. Rev.*, 2015, **44**, 1379–1415.
4 G. Chen, H. Ågren, T. Y. Ohulchanskyy and P. N. Prasad, *Chem. Soc. Rev.*, 2015, **44**, 1680–1713.
5 X. Ai, Z. Wang, H. Cheong, Y. Wang, R. Zhang, J. Lin, Y. Zheng, M. Gao and B. Xing, *Nat. Commun.*, 2019, **10**, 1087.
6 V. Marturano, J. Kozlowska, A. Bajek, M. Giamberini, V. Ambrogi, P. Cerruti, R. Garcia-Valls, J. M. Montornes and B. Tylkowski, *Coord. Chem. Rev.*, 2019, **398**, 213013.
7 L. Sun, R. Wei, J. Feng and H. Zhang, *Coord. Chem. Rev.*, 2018, **364**, 10–32.
8 J. C. Goldschmidt and S. Fischer, *Adv. Opt. Mater.*, 2015, **3**, 510–535.

9 B. Chen, W. Kong, Y. Liu, Y. Lu, M. Li, X. Qiao, X. Fan and F. Wang, *Angew. Chem., Int. Ed.*, 2017, **56**, 10383–10387.
10 N. M. Idris, M. K. G. Jayakumar, A. Bansal and Y. Zhang, *Chem. Soc. Rev.*, 2015, **44**, 1449–1478.
11 G. Tessitore, S. L. Maurizio, T. Sabri and J. A. Capobianco, *Angew. Chem., Int. Ed.*, 2019, **58**, 9742–9751.
12 B. Tian, A. Fernandez-Bravo, H. Najafiaghdam, N. A. Torquato, M. V. P. Altoe, A. Teitelboim, C. A. Tajon, Y. Tian, N. J. Borys, E. S. Barnard, M. Anwar, E. M. Chan, P. J. Schuck and B. E. Cohen, *Nat. Commun.*, 2018, **9**, 3082.
13 G. Jalani, V. Tam, F. Vetrone and M. Cerruti, *J. Am. Chem. Soc.*, 2018, **140**, 10923–10931.
14 S. Fischer, R. D. Mehlenbacher, A. Lay, C. Siefe, A. P. Alivisatos and J. A. Dionne, *Nano Lett.*, 2019, **19**, 3878–3885.
15 M. Haase and H. Schäfer, *Angew. Chem., Int. Ed.*, 2011, **50**, 5808–5829.
16 J. Ueda, P. Dorenbos, A. J. Bos, A. Meijerink and S. Tanabe, *J. Phys. Chem. C*, 2015, **119**, 25003–25008.
17 A. Taguchi, H. Nakagome and K. Takahei, *J. Appl. Phys.*, 1991, **70**, 5604–5607.
18 J. Lambkin, D. Dunstan, K. Homewood, L. Howard and M. Emeny, *Appl. Phys. Lett.*, 1990, **57**, 1986–1988.
19 B. Cao, Y. Bao, Y. Liu, J. Shang, Z. Zhang, Y. He, Z. Feng and B. Dong, *Chem. Eng. J.*, 2020, **385**, 123906.
20 D. Li, W.-Y. Lai, X. Shen, Q. Shao and W. Huang, *Mater. Chem. Front.*, 2019, **3**, 791–795.
21 L. Li, F. Qin, Y. Zhou, Y. Zheng, H. Zhao and Z. Zhang, *J. Lumin.*, 2019, **206**, 335–341.
22 T. Pang, W. Peng, M. Yang, J. Xie and W. Lu, *J. Rare Earths*, 2018, **36**, 1136–1140.
23 Q. Han, W. Gao, J. Qi, X. Zhao, J. Zhang, Y. Wang, S. Dong, W. Liu, A. Hao and J. Dong, *J. Lumin.*, 2019, **212**, 227–232.
24 R. Luo, Q. Li, J. Wang, Z. Ning, Y. Zhao, M. Liu, X. Lai, C. Zhong, J. Bi and D. Gao, *J. Alloys Compd.*, 2020, **828**, 154375.
25 P. Du and J. S. Yu, *Curr. Appl. Phys.*, 2017, **17**, 1662–1669.
26 K. Zheng, Z. Liu, C. Lv and W. Qin, *J. Mater. Chem. C*, 2013, **1**, 5502–5507.
27 Z. Wang, P. Zhang, Q. Yuan, X. Xu, P. Lei, X. Liu, Y. Su, L. Dong, J. Feng and H. Zhang, *Nanoscale*, 2015, **7**, 17861–17870.
28 K. Zheng, G. He, W. Song, X. Bi and W. Qin, *J. Mater. Chem. C*, 2015, **3**, 11589–11594.
29 A. Yakovliev, T. Y. Ohulchanskyy, R. Ziniuk, T. Dias, X. Wang, H. Xu, G. Chen, J. Qu and A. S. Gomes, *Part. Part. Syst. Charact.*, 2020, **37**, 1900445.
30 M. Ding, C. Lu, L. Chen and Z. Ji, *J. Alloys Compd.*, 2018, **763**, 85–93.
31 X. Bai, H. Song, G. Pan, Y. Lei, T. Wang, X. Ren, S. Lu, B. Dong, Q. Dai and L. Fan, *J. Phys. Chem. C*, 2007, **111**, 13611–13617.
32 L. Li, F. Qin, L. Li, H. Gao and Z. Zhang, *J. Mater. Chem. C*, 2019, **7**, 7378–7385.
33 W. Xu, Y. Hu, L. Zheng, Z. Zhang and W. Cao, *J. Lumin.*, 2019, **215**, 116617.
34 K. W. Meert, V. A. Morozov, A. M. Abakumov, J. Hadermann, D. Poelman and P. F. Smet, *Opt. Express*, 2014, **22**, A961–A972.
35 E.-H. Song, S. Ding, M. Wu, S. Ye, F. Xiao, G.-P. Dong and Q.-Y. Zhang, *J. Mater. Chem. C*, 2013, **1**, 4209–4215.
36 Z. Chen, E. Song, M. Wu, S. Ding, S. Ye and Q. Zhang, *J. Alloys Compd.*, 2016, **667**, 134–140.
37 Y. Li, Z. Li, L. Guo, B. Yang and T. Li, *J. Alloys Compd.*, 2020, **847**, 156399.
38 P. Du, Y. Guo, S. H. Lee and J. S. Yu, *RSC Adv.*, 2017, **7**, 3170–3178.
39 D. Chen, S. Liu, X. Li, S. Yuan and P. Huang, *J. Eur. Ceram. Soc.*, 2017, **37**, 4939–4945.
40 H. Guan, Y. Sheng, Y. Song, C. Xu, X. Zhou, K. Zheng, Z. Shi and H. Zou, *J. Phys. Chem. C*, 2017, **121**, 23080–23095.
41 B. Chen and F. Wang, *Trends Chem.*, 2020, **2**, 427–439.
42 M. Weber, *Phys. Rev. B: Solid State*, 1973, **8**, 54.
43 D. Yu, T. Yu, Y. Wang, Q. Zhang and A. Meijerink, *Phys. Rev. Appl.*, 2020, **13**, 024076.
44 D. Yu, J. Ballato and R. E. Riman, *J. Phys. Chem. C*, 2016, **120**, 9958–9964.
45 E. C. Ximendes, A. F. Pereira, U. Rocha, W. F. Silva, D. Jaque and C. Jacinto, *Nanoscale*, 2019, **11**, 8864–8869.
46 J. M. F. van Dijk and M. F. H. Schuurmans, *J. Chem. Phys.*, 1983, **78**, 5317–5323.
47 L. A. Riseberg and H.-W. Moos, *Phys. Rev.*, 1968, **174**, 429.
48 Y. Zhao, C. Riemersma, F. Pietra, R. Koole, C. de Mello Donegá and A. Meijerink, *ACS Nano*, 2012, **6**, 9058–9067.
49 M. Lax, *J. Chem. Phys.*, 1952, **20**, 1752–1760.
50 J. Ueda, A. Meijerink, P. Dorenbos, A. J. Bos and S. Tanabe, *Phys. Rev. B*, 2017, **95**, 014303.
51 A. D'Aléo, F. Pointillart, L. Ouahab, C. Andraud and O. Maury, *Coord. Chem. Rev.*, 2012, **256**, 1604–1620.
52 H. Hoefdraad, *J. Inorg. Nucl. Chem.*, 1975, **37**, 1917–1921.
53 P. Dorenbos, *J. Phys.: Condens. Matter*, 2003, **15**, 4797.
54 J. J. Joos, L. Seijo and Z. Barandiarán, *J. Phys. Chem. Lett.*, 2019, **10**, 1581–1586.
55 B. Chen, X. Qiao, D. Peng and X. Fan, *J. Phys. Chem. C*, 2014, **118**, 30197–30201.
56 F. Wang and X. Liu, *Acc. Chem. Res.*, 2014, **47**, 1378–1385.
57 T. Forster, *Ann. Phys.*, 1948, **2**, 55–75.
58 D. L. Dexter, *J. Chem. Phys.*, 1953, **21**, 836–850.
59 B. Chen, Q. Su, W. Kong, Y. Wang, P. Shi and F. Wang, *J. Mater. Chem. B*, 2018, **6**, 2924–2944.
60 B. Henderson and G. F. Imbusch, *Optical spectroscopy of inorganic solids*, Oxford Science Publications, London, 2006.
61 X. Chen, D. Peng, Q. Ju and F. Wang, *Chem. Soc. Rev.*, 2015, **44**, 1318–1330.
62 T. Sun, Y. Li, W. L. Ho, Q. Zhu, X. Chen, L. Jin, H. Zhu, B. Huang, J. Lin, B. E. Little, S. T. Chu and F. Wang, *Nat. Commun.*, 2019, **10**, 1811.

63 D. L. Dexter and J. H. Schulman, *J. Chem. Phys.*, 1954, **22**, 1063–1070.
64 R. Arppe, I. Hyppänen, N. Perälä, R. Peltomaa, M. Kaiser, C. Würth, S. Christ, U. Resch-Genger, M. Schäferling and T. Soukka, *Nanoscale*, 2015, **7**, 11746–11757.
65 B. Chen and F. Wang, *Acc. Chem. Res.*, 2019, **53**, 358–367.
66 F. Wang, J. Wang and X. Liu, *Angew. Chem., Int. Ed.*, 2010, **49**, 7456–7460.
67 B. Chen and F. Wang, *Inorg. Chem. Front.*, 2020, **7**, 1067–1081.
68 S. Guo, X. Xie, L. Huang and W. Huang, *ACS Appl. Mater. Interfaces*, 2016, **8**, 847–853.
69 R. Shi, E. D. Martinez, C. D. S. Britesa and L. D. Carlos, *Phys. Chem. Chem. Phys.*, 2021, **23**, 20–42.
70 Y. Hu, Q. Shao, P. Zhang, Y. Dong, F. Fang and J. Jiang, *J. Phys. Chem. C*, 2018, **122**, 26142–26152.
71 Z. Wang, J. Christiansen, D. Wezendonk, X. Xie, M. A. Van Huis and A. Meijerink, *Nanoscale*, 2019, **11**, 12188–12197.
72 Y. Hu, Q. Shao, X. Deng and J. Jiang, *Nanophotonics*, 2020, **9**, 2879–2885.
73 Q. Chen, X. Xie, B. Huang, L. Liang, S. Han, Z. Yi, Y. Wang, Y. Li, D. Fan and L. Huang, *Angew. Chem., Int. Ed.*, 2017, **56**, 7605–7609.
74 Q. Su, S. Han, X. Xie, H. Zhu, H. Chen, C.-K. Chen, R.-S. Liu, X. Chen, F. Wang and X. Liu, *J. Am. Chem. Soc.*, 2012, **134**, 20849–20857.
75 L. Liang, X. Qin, K. Zheng and X. Liu, *Acc. Chem. Res.*, 2018, **52**, 228–236.
76 F. Wang, R. Deng, J. Wang, Q. Wang, Y. Han, H. Zhu, X. Chen and X. Liu, *Nat. Mater.*, 2011, **10**, 968–973.
77 X. Cui, Y. Cheng, H. Lin, F. Huang, Q. Wu and Y. Wang, *Nanoscale*, 2017, **9**, 13794–13799.
78 B. Chen, W. Kong, N. Wang, G. Zhu and F. Wang, *Chem. Mater.*, 2019, **31**, 4779–4786.
79 D. Li, Q. Shao, Y. Dong and J. Jiang, *J. Phys. Chem. C*, 2014, **118**, 22807–22813.
80 E. D. Martínez, C. D. Brites, L. D. Carlos, A. F. García–Flores, R. R. Urbano and C. Rettori, *Adv. Funct. Mater.*, 2019, **29**, 1807758.
81 Q. Shao, G. Zhang, L. Ouyang, Y. Hu, Y. Dong and J. Jiang, *Nanoscale*, 2017, **9**, 12132–12141.
82 D. D. Li, Q. Y. Shao, Y. Dong, F. Fang and J. Q. Jiang, *Part. Part. Syst. Charact.*, 2015, **32**, 728–733.
83 L. Lei, D. Chen, C. Li, F. Huang, J. Zhang and S. Xu, *J. Mater. Chem. C*, 2018, **6**, 5427–5433.
84 C. D. Brites, E. D. Martínez, R. R. Urbano, C. Rettori and L. D. Carlos, *Front. Chem.*, 2019, **7**, 267.
85 E. D. Martínez, R. R. Urbano and C. Rettori, *ACS Appl. Nano Mater.*, 2019, **2**, 6889–6897.
86 L. Lei, J. Xia, Y. Cheng, Y. Wang, G. Bai, H. Xia and S. Xu, *J. Mater. Chem. C*, 2018, **6**, 11587–11592.
87 D. Baek, T. K. Lee, I. Jeon, S. H. Joo, S. Shin, J. Park, S. J. Kang, S. K. Kwak and J. Lee, *Adv. Sci.*, 2020, **7**, 2000104.
88 Y. Hu, Q. Shao, X. Deng, D. Song, S. Han, Y. Dong and J. Jiang, *J. Mater. Chem. C*, 2019, **7**, 11770–11775.
89 C. Mi, J. Zhou, F. Wang, G. Lin and D. Jin, *Chem. Mater.*, 2019, **31**, 9480–9487.
90 Y. Hu, Q. Shao, X. Deng, S. Han, D. Song and J. Jiang, *Adv. Mater. Technol.*, 2019, **4**, 1800498.
91 J. Suyver, J. Grimm, K. Krämer and H.-U. Güdel, *J. Lumin.*, 2005, **114**, 53–59.
92 G. Salley, R. Valiente and H. Guedel, *J. Lumin.*, 2001, **94**, 305–309.
93 X. Xu, W. Zhang, D. Yang, W. Lu, J. Qiu and S. F. Yu, *Adv. Mater.*, 2016, **28**, 8045–8050.
94 X. Chen, H. Zhuang, G. Liu, S. Li and R. Niedbala, *J. Appl. Phys.*, 2003, **94**, 5559–5565.
95 G. Liu, H. Zhuang and X. Chen, *Nano Lett.*, 2002, **2**, 535–539.
96 J. Zhou, S. Wen, J. Liao, C. Clarke, S. A. Tawfik, W. Ren, C. Mi, F. Wang and D. Jin, *Nat. Photonics*, 2018, **12**, 154.
97 T. Varga, A. P. Wilkinson, C. Lind, W. A. Bassett and C.-S. Zha, *J. Phys.: Condens. Matter*, 2005, **17**, 4271.
98 W. Miller, C. Smith, D. Mackenzie and K. Evans, *J. Mater. Sci.*, 2009, **44**, 5441–5451.
99 H. Liu, W. Sun, Z. Zhang, X. Zhang, Y. Zhou, J. Zhu and X. Zeng, *Inorg. Chem. Front.*, 2019, **6**, 1842–1850.
100 R. Zhu, K. Jia, Z. Bi, Y. Liu and Y. Lyu, *J. Solid State Chem.*, 2020, **290**, 121592.
101 H. Zou, X. Yang, B. Chen, Y. Du, B. Ren, X. Sun, X. Qiao, Q. Zhang and F. Wang, *Angew. Chem., Int. Ed.*, 2019, **58**, 17255–17259.
102 H. Zou, B. Chen, Y. Hu, Q. Zhang, X. Wang and F. Wang, *J. Phys. Chem. Lett.*, 2020, **11**, 3020–3024.
103 B. Ren, B. Chen, J. Zhao, Y. Guo, X. Zhang, X. Chen, Y. Du, Z. Deng, G. Zhu and F. Wang, *Chem. Mater.*, 2021, **33**, 158–163.
104 Y. H. Kim, P. Arunkumar, B. Y. Kim, S. Unithrattil, E. Kim, S.-H. Moon, J. Y. Hyun, K. H. Kim, D. Lee, J.-S. Lee and W. B. Im, *Nat. Mater.*, 2017, **16**, 543–550.
105 Z. Tang, G. Zhang and Y. Wang, *ACS Photonics*, 2018, **5**, 3801–3813.
106 J. Qiao, L. Ning, M. S. Molokeev, Y.-C. Chuang, Q. Liu and Z. Xia, *J. Am. Chem. Soc.*, 2018, **140**, 9730–9736.
107 J. Wen, Z. Guo, H. Guo, L. Ning, C.-K. Duan, Y. Huang, S. Zhan and M. Yin, *Inorg. Chem.*, 2018, **57**, 6142–6151.
108 R. Shi, L. Ning, Z. Wang, J. Chen, T. K. Sham, Y. Huang, Z. Qi, C. Li, Q. Tang and H. Liang, *Adv. Opt. Mater.*, 2019, **7**, 1901187.
109 Y. Chen, B. Yu, J. Gou and S. F. Liu, *J. Mater. Chem. C*, 2018, **6**, 10687–10692.
110 L. Wang, X. Li, Z. Li, W. Chu, R. Li, K. Lin, H. Qian, Y. Wang, C. Wu, J. Li, D. Tu, Q. Zhang, L. Song, J. Jiang, X. Chen, Y. Xie and Y. Xiong, *Adv. Mater.*, 2015, **27**, 5528–5533.
111 Z. Wang, X. Li, G. Zhang, Y. Luo and J. Jiang, *ACS Appl. Mater. Interfaces*, 2017, **9**, 23309–23313.
112 B. Chen, Y. Wang, Y. Guo, P. Shi and F. Wang, *ACS Appl. Mater. Interfaces*, 2021, **13**, 2327–2335.
113 J. Zhao, X. Chen, B. Chen, X. Luo, T. Sun, W. Zhang, C. Wang, J. Lin, D. Su, X. Qiao and F. Wang, *Adv. Funct. Mater.*, 2019, **29**, 1903295.

114 N. J. Johnson and F. C. van Veggel, *ACS Nano*, 2014, **8**, 10517–10527.
115 J. Zhao, B. Chen and F. Wang, *Adv. Mater.*, 2020, 2004142.
116 S. J. Baxter, B. R. Hester, B. R. Wright and A. P. Wilkinson, *Chem. Mater.*, 2019, **31**, 3440–3448.
117 J. C. Hancock, K. W. Chapman, G. J. Halder, C. R. Morelock, B. S. Kaplan, L. C. Gallington, A. Bongiorno, C. Han, S. Zhou and A. P. Wilkinson, *Chem. Mater.*, 2015, **27**, 3912–3918.
118 D. J. Fisher, *Negative Thermal Expansion Materials*, Materials Research Forum LLC, Millersville, 2018.